J. Mt. Sci. (2019) 16(1): 108-121 e-mail: jms@imde.ac.cn http://jms.imde.ac.cn
https://doi.org/10.1007/s11629-018-4989-z

Formation conditions of landslide dams triggered by incision of mine waste accumulations

ZHU Xing-hua[1,2] http://orcid.org/0000-0002-3935-6288; e-mail: zhuxinghua@chd.edu.cn

PENG Jian-bing[1,2*] http://orcid.org/0000-0003-4689-7717; e-mail: oldbig2130@163.com

JIANG Cheng[3] http://orcid.org/0000-0001-7654-0933; e-mail: 1228384952@qq.com

GUO Wei-long[1,2] http://orcid.org/0000-0001-5199-1359; e-mail: 756634350@qq.com

** Corresponding author*

1 College of Geological Engineering and Surveying, Chang'an University, Xi'an 710054, China

2 Key Laboratory of Western China Mineral Resources and Geological Engineering, Chang'an University, Xi'an 710054, China

3 School of Environmental Science and Engineering, Chang'an University, Xi'an 710054, China

Citation: Zhu XH, Peng JB, Jiang C, et al. (2019) Formation conditions of landslide dams triggered by incision of mine waste accumulations. Journal of Mountain Science 16(1). https://doi.org/10.1007/s11629-018-4989-z

Abstract: The erosion and delivery processes of mine waste accumulations were reproduced through flume tests under 13 different experimental condition sets. Analysis of the flume test results showed that different scale model landslides, induced by the incision of mine waste accumulations, slipped into the channel and caused complete or partial blockages, with 28 complete blockages and 122 partial blockages observed during the flume tests. The failure of these temporary landslide dams amplified the peak discharge significantly, with the amplification more obvious when caused by the failure of a complete blockage compared to a partial blockage under the same experimental conditions. In order to explore the threshold conditions of a complete blockage, a new blockage index (I_{bs}) was developed to represent the degree of blockage. It was found that the threshold value of the blockage index for a complete blockage was around I_{bs}=4.0. What's more, there was a significant negative correlation between the blockage index and the amplification coefficient of peak discharge caused by the failure of a landslide dam. These preliminary results are intended to provide a scientific basis for future research on the disaster prevention and mitigation of mine waste debris flows, as the processes and mechanisms underlying the erosion and delivery of mine waste accumulations by upstream flows along a gully have not yet been clearly identified.

Key words: Mine waste; Landslide dams; Complete blockage; Partial blockage; Blockage index

Received: 18 April 2018
Revised: 26 October 2018
Accepted: 3 December 2018

Introduction

A landslide dam is formed when an unconsolidated heterogeneous mixture of earth or rock debris reaches the bottom of a river valley and causes a complete or partial blockage (Costa and Schulter 1988; Ermini and Casagli 2003). Subsequently, an impoundment may be formed upstream in either instance (Casagli and Ermini 1999). Landslide dams are always unstable, and 85% fail within one year of formation (Costa and Schuster 1988). The formation and failure of landslide dams can cause extremely consequential disasters such as catastrophic outburst floods, debris flows, and backwater ponding (Korup 2005; Dong et al. 2009), particularly when a flow from upstream to downstream crushes an obstructive landslide dam at high speed and incises it rapidly. When this occurs, sediment delivery of the landslide debris is considerable and debris flows are easily formed. A large number of catastrophic debris flows have originated in this manner (Lombard et al. 1981; Gallino and Pierson 1984; King et al. 1989; Cenderelli and Kite 1998).

A considerable number of important research achievements concerning landslide dams have been made in recent years. Based on a landslide dam's geometric relationship with a valley floor, Swanson et al. (1986) proposed a geomorphic classification scheme for the dams. Soon afterwards, this scheme was modified by Costa and Schuster (1988, 1991), who classified six types of landslide dams. Based on a dataset of 184 case studies, it was found that natural dams were mainly the first three types: Type I dams are small in contrast to the width of the valley floor and do not reach from one valley side to the other; Type II dams are larger and span the entire valley floor; Type III dams fill the valley from side to side, move considerable distances upper valley and lower valley from the failure, and typically involve the largest volume of landslide material. In their classification system, landslide dams that blocked a channel completely (including Type II and Type III) accounted for 85% of all landslide dams, while partial blockage (Type I) accounted for 11% of landslide dams, with the other 4 types being quite rare. In recent years, some scholars have focused on quantitative methods for determining post-formation development, in particular studying the controls affecting dam longevity (Ermini and Casagli 2003; Korup 2002, 2004, 2005; Schuster 2000).

Since there has been only a very few landslide dams for which their formation and failure have been directly observed, very little is known about these actual processes. Therefore, several mathematical models have been developed to simulate the failure process of such dams and the resulting outburst discharge (Brown and Rogers 1977; Fread 1977; Ponce and Yevjevich 1978; Singh et al. 1986). Some scholars used the discrete element method (DEM) to simulate the failure process as DEM offers unique advantages in modeling discontinuous materials (Cui et al. 2017a, 2017b), which rely on the development of DEM and fluid flow coupling (Cui et al. 2016) to represent the mechanical behavior of during entrainment process. However, there is surprisingly little mention of the formation conditions involved that enable a landslide to cause both a temporal and spatial blockage of a river flow (Korup 2002), in spite of its significance to hazard prevention and mitigation. Damming is a complex process that involves the volume and speed of mass movement combined with the geomorphic parameters of valley floor/ channel geometry and hydrologic variables such as discharge, stream power, and/or flow resistance (Costa and Schuster 1988; Casagli and Ermini 1999; Korup 2002).

The Xiaoqinling gold mining area is located at the junction of Shaanxi Province and Henan Province in China. Over the last few decades, a large amount of mine waste produced during the gold mining process has been stacked in disorderly fashion along the gullies in the region, which have subsequently become sources of debris flows. At present, there are now quite a number of high-frequency debris flow gullies distributed throughout the area, and debris flows often occur. In particular, a catastrophic debris flow was triggered by heavy rainfall in the Daxicha Gully on July 11, 1994. According to a field investigation conducted by Li (1995), the peak discharge of the debris flow was amplified more than 2,000 times over usual flow volumes due to blockages created by abandoned mine waste. The peak discharge of the debris flow was 260 m^3/s with a 5m depth, and resulted in 51 deaths, more than 2,000 others missing, and economic losses of more than 17 million yuan (Li 1995; Liu et al. 1996). In recent years, several other subsequent debris flows have occurred in the same gully (Liu et al. 1996; Deng et al. 2009).

For this work, field investigations in the Xiaoqinling mining area were conducted three times in 2016 and 2017,which found a significant number of mine waste piles - some more than 30 meters in height and with a slope of close to 40 degrees - distributed along the channel (Figure 1(a)). Clearly, the problem of haphazard stacking of mine waste has not been effectively controlled in

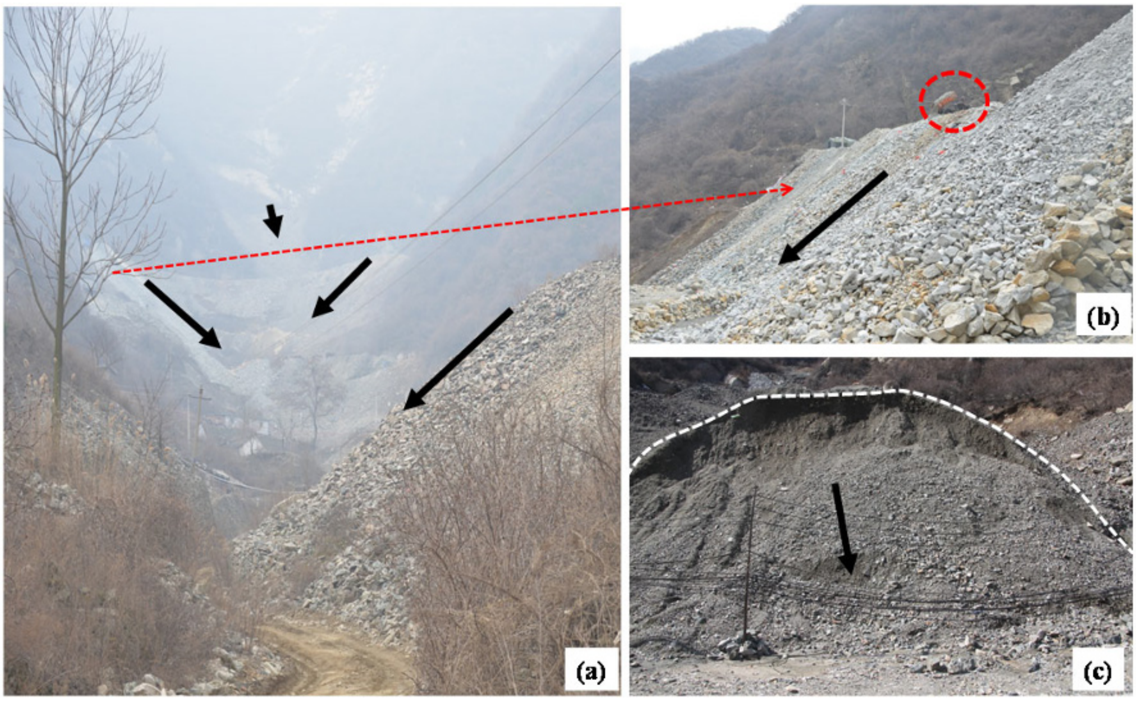

Figure 1 Mine waste accumulations in the Daxicha Gully.

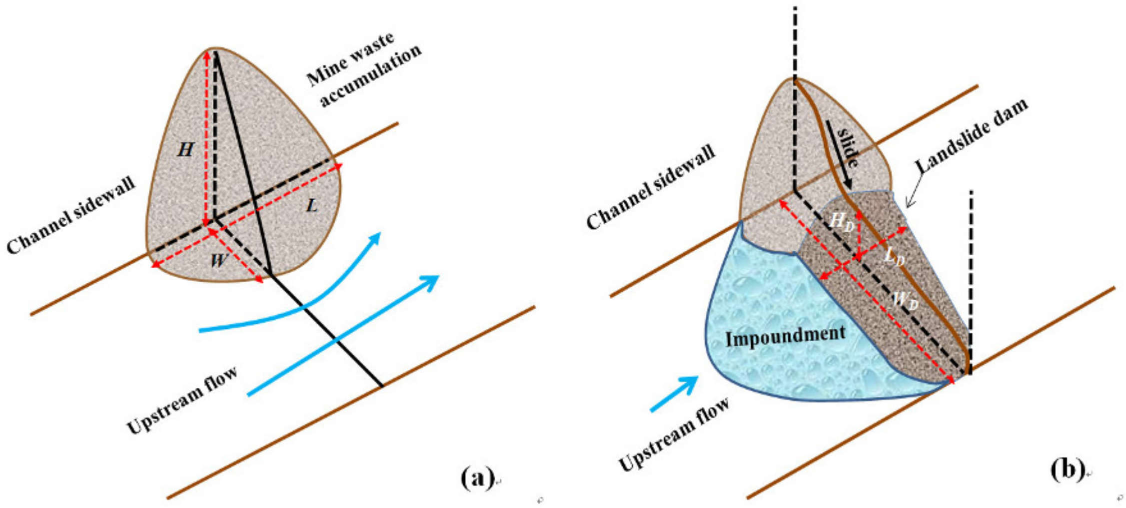

Figure 2 Erosion and delivery processes of mine waste in a channel.

this region. Figure 1(b) is a partial enlargement of a mine waste accumulation shown on the left side of Figure 1(a), which depicts a dump truck dumping mine waste onto the pile. As the loose mine waste is coarse and possesses high permeability, the slope of such mine waste accumulations is continually destabilized by rainfall or runoff (Figure 1(c)). Based on these detailed field investigations along the Daxicha Gully, it can be inferred that if a flash flood forms in the catchment area upstream, it will strongly scour the toes of the mine waste accumulations along the channel (Figure 2(a)). This could cause a large volume of loose mine waste to either be delivered swiftly along the gully or slip into the channel induced by the strong incision of the mine waste accumulations and form landslide dams (Figure 2(b)).The peak discharge of floods (or debris flow) would then be significantly amplified due to the formation and failure of these temporary landslide dams. The "magnification effect" in this process has been confirmed by both field surveys and model experiments (Cui et al.

2013; Zhou et al. 2013; Chen et al. 2014; Hu et al. 2015).

To understand this important process, flume tests were conducted to reproduce the formation and failure processes of landslide dams. By analyzing the results of the flume tests, this paper aims to infer the formation conditions of landslide dams triggered by the incision of mine waste accumulation, which can in turn be a scientific basis for future research.

1 Experimental Method

1.1 Experimental setup

Based on the data accumulated from field investigations of the Daxicha Gully in the Xiaoqinling gold mining area, an experimental model was designed. In principle, the scaled reproduction of incision of mine wastes accumulations along the flume should adhere to correct geometric, kinematic, and dynamic scale ratios between the model and prototype. However, not all relationships can be satisfied simultaneously in model tests (e.g., gravel sized materials cannot be scaled into sand sized materials since they don't share the same characteristics). In our experiments, for free-surface flows dominated by gravitational and inertial forces, Froudian model scaling laws (λ_F=1) should be obeyed to maintain dynamic flow similarity. Where λ_F =1 is the scale ratio of Froude number $F=U/(gL)^{0.5}$, U is flow velocity, g is gravitational acceleration, and L is the governing length for the phenomenon. λ_g=1, λ_F=1 implies scaling ratios for velocity, time and flow rate of $\lambda_U=\lambda_L^{0.5}$, $\lambda_t=\lambda_L/\lambda_U=\lambda_U^{0.5}$,$\lambda_Q=\lambda_U\lambda_A=\lambda_L^{2.5}$ as well as the roughness scaling is $\lambda_n=\lambda_L^{0.17}$ respectively. The experimental flume was designed with scale ratio of λ_L=100. Figure 3 shows an overview of the experimental setup, which includes a water tank, flume, and tailings pond. The storage tank is 1.3 m in length, 1.3 m in width, and 1.8m in height. Water was sent directly into the upper part of the flume through a water pump installed on the left side of the tank. At the middle of the pipeline, an electromagnetic flowmeter combined with a flow-balancing valve was used to accurately control the flow rate of water. A triangular weir, installed upstream of the flume, was used to adjust flow stability. The flume is 4m in length, 0.3 m in width and 0.5 m in height. The bottom of the flume is rough steel plate and the two sides are tempered glass, which made it convenient to observe the erosion and delivery processes of mine waste. The slope of the flume could be easily adjusted between 6° and 35°. The tailings pond

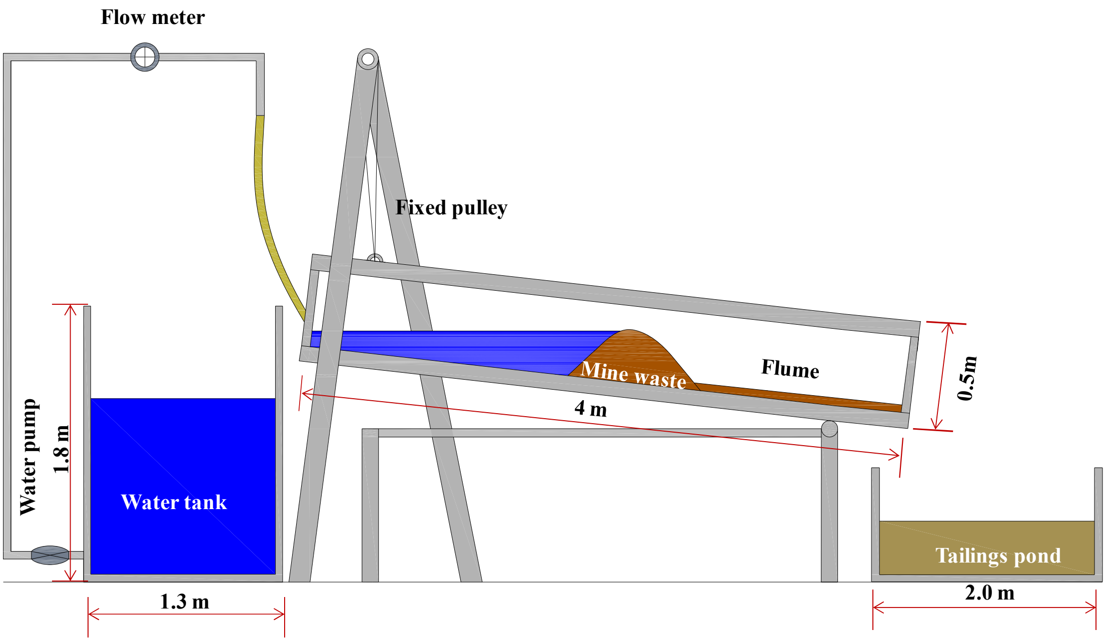

Figure 3 Sketch of the experimental setup.

was used to collect experimental tailings.

1.2 Experiment design

The mine waste material used for the flume tests was all taken from mine waste dumps in the Daxicha Gully. The gradings of the in situ sample and the material for the flume test are shown in Figure 4. It can be seen from the grading of sample in situ in Figure 4, the proportion of fine particles below 2 mm is less than 10%, while the coarse particles larger than 50 mm are more than 65%. Moreover, the particles of mine waste almost have low psephicity. Due to the grading characteristics of mine waste mentioned above, the mine waste accumulations are always in the condition of large porosity and high permeability. However, to take into account the hydrodynamic conditions of the experimental setup, particles larger than 5 cm were removed from the collected material.

It was found that the slope of the debris flow stacking fan is about 5° in situ, so the slope of the flume tests should be no less than 5°. When the flow rate is 0.0015 m³/s, we carried out 8 tests under different slopes. There were significant differences in the transport mode of mine wastes under different gradients when the slope was less than 10°. However, when the slope was greater than 10°, nearly all of the mine wastes can be transported. When the flow rate reached to 0.002 m³/s and 0.0025 m³/s, the mine wastes were all transported quickly even under different gradients. Therefore, a total of 13 different test conditions in our research were conducted and shown in Table 1. Before every test, the slope angle and upstream flow rate were accurately adjusted and then mine wastes tacked according to the sizes listed in Table 1. The flume was 4 m in length (in Figure 3). In the first 2 meters, the flow from upstream can be greatly accelerated. All waste accumulations of each test was located in the third meter. The forth meter has been used to steady the flow, and to measure the average flow depth in cross section at the end of the flume. The processes of every tests were recorded by three cameras from the front, the right side, and the top. A metric ruler was placed

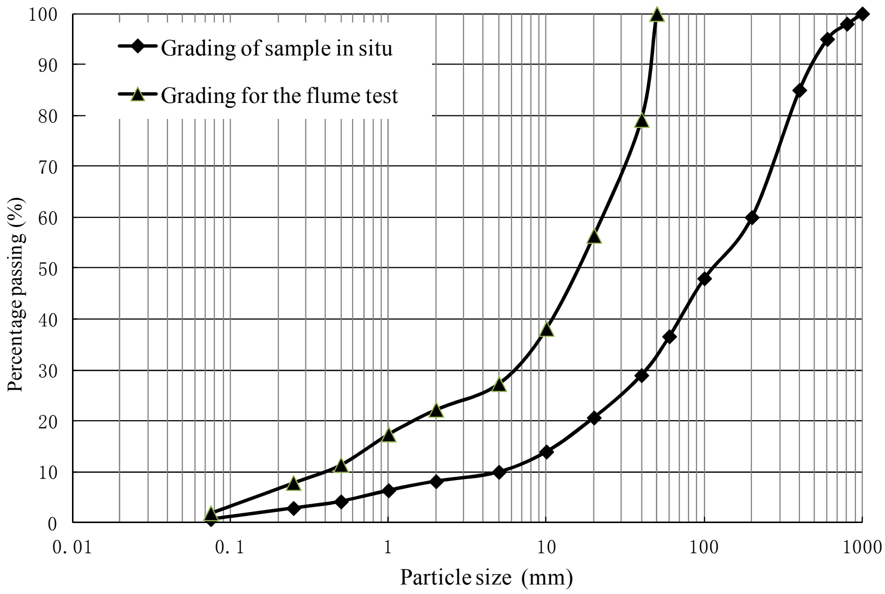

Figure 4 Particle size distribution of the modeled mine waste and the in situ particle size

Table 1 Summary of parameters for the 13 experimental tests

No.	Characteristics of modeled mine waste accumulation				θ (°)	Q_o (m³/s)
	V_t (m³)	H (m)	W (m)	L (m)		
1	0.0200	0.26	0.28	0.98	5	0.0015
2	0.0142	0.29	0.27	0.93	6	0.0015
3	0.0139	0.25	0.28	0.99	7	0.0015
4	0.0125	0.25	0.25	0.83	8	0.0015
5	0.0170	0.25	0.28	0.93	9	0.0015
6	0.0181	0.29	0.23	1.02	10	0.0015
7	0.0137	0.27	0.23	1.01	12	0.0015
8	0.0104	0.24	0.26	0.95	15	0.0015
9	0.0182	0.29	0.27	0.88	5	0.0020
10	0.0128	0.26	0.27	1.01	7	0.0020
11	0.0162	0.27	0.27	1.03	9	0.0020
12	0.0118	0.27	0.25	0.95	5	0.0025
13	0.0168	0.28	0.26	1.01	7	0.0025

Notes: V_t is the total volume of the mine waste accumulation, θ is the slope angle, and Q_o is the inflow discharge, H, W and L are the height, width and length of mine waste accumulation (in Figure 2(a)).

on the right side of the flume to measure flow depth downstream. In order to determine the flow velocity downstream of the mine waste heap, a float method was adopted based on the videos provided by three cameras at the speed of 25 frames per second. Thus we can calculate average speed of every 0.04 seconds by using the size scale marked on the flume. The method was calibrated before our experiments, and the average error was less than 5%.

2 Results and Discussion

Analysis of the results from the 13 model tests showed that the erosion and delivery processes of the mine waste accumulations in the flume could be divided into several stages, which can be seen in Figure 5. Due to the continuous erosion and delivery of material at the toe of the mine waste accumulation created for each test, landslides would form and slip into the flume instantaneously. Some of these debris slides are immediately delivered by the flow from upstream (Figure 5(a)), while others cause a partial (Figure 5(b)) or complete blockage (Figure 5(c)), forming an impoundment upstream in both instances. The damming and breaching effect of these temporary dams significantly amplifies the peak discharge (Figure 5(d)), known as the amplification effect (Cui et al. 2013; Zhou et al. 2013; Chen et al. 2014; Hu et al. 2015).

The results of these flume tests show that not all debris slides result in the blockage of a river channel. Such a blockage only occurs in instances where a large amount of material can be moved with high velocity (Ermini and Casagli 2003). Therefore, we can speculate that there must be a scaling threshold, and any mass movement exceeding the threshold may cause a blockage, while mass movement below the threshold can only be swiftly delivered by the flow from upstream. However, the models correlating landslide volume, fall height, and runout distance are mostly based on data from specific landslide events, and none have been widely recognized as a universal explanation for landslide mobility (Straub 1997; Legros 2002). Therefore, it is difficult to find a model suitable for analyzing the experimental data gathered in this work. However, for the convenience of this experimental data analysis, three rules were followed:

(1) Since the width of the flume was 0.3 m, the scaling threshold of the blockages mentioned above was assumed to be 30×10^{-5} m^3. In the 13 flume tests, all of the landslides with a volume of less than 30 cm^3 were assumed to have not blocked the flume or formed an impounding.

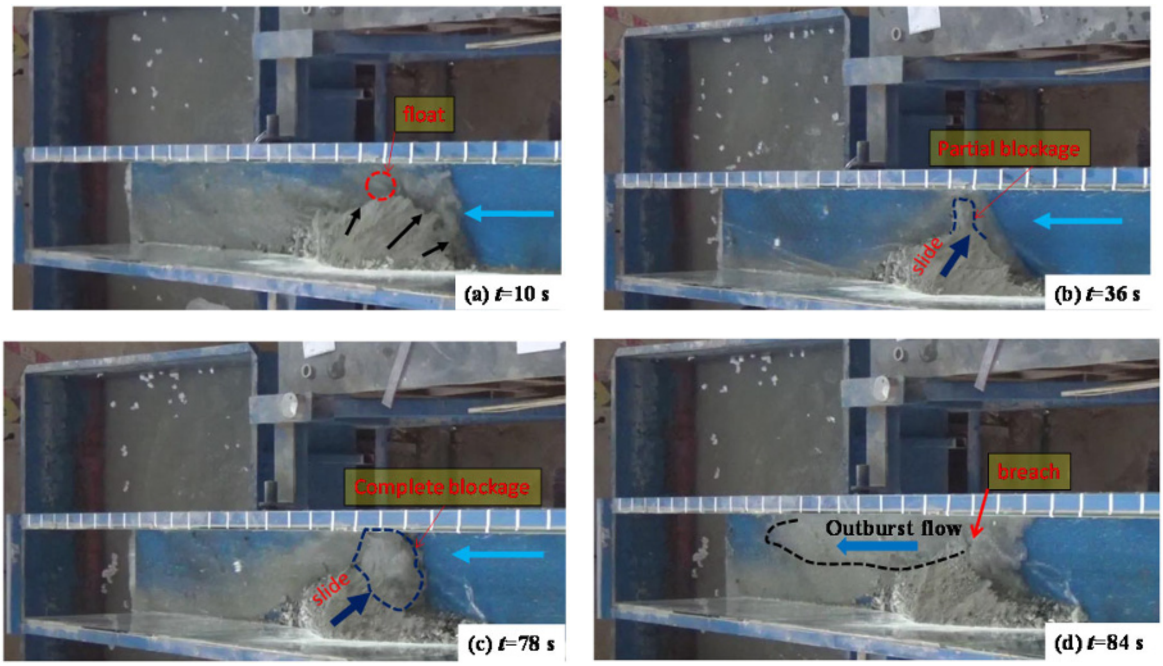

Figure 5 The delivery process of mine waste in the flume (Q_0=1.5 L/s, θ=7^{0}).

Table 2 All partial and complete blockages for each experiment

(θ, Q_o) (°, m^3/s)	t(s)	TB	V_m (cm^3)	Q_{out} (cm^3)	m	(θ, Q_o) (°, m^3/s)	t(s)	TB	V_m (cm^3)	Q_{out} (cm^3)	m
(5, 0.0015)	49	PB	78.75	1701	1.13	(5, 0.002)	193	PB	534.4	2556	1.28
	61	CB	221	2430	1.62		195	PB	133.33	2130	1.07
	101	PB	84	1704	1.14		202	PB	86.1	2079	1.04
	158	CB	444	3024	2.02		205	PB	478.5	2343	1.17
(6, 0.0015)	32	PB	561	2772	1.85		211	PB	252	2130	1.07
	42	CB	764	3276	2.18		219	PB	120.56	2079	1.04
	80	CB	589.6	3003	2.00		225	PB	396	2343	1.17
	105	CB	666	3276	2.18		230	PB	260.3	2130	1.07
	164	PB	127.8	1704	1.14		240	PB	52	2079	1.04
(7, 0.0015)	36	PB	68.64	1704	1.14	(7, 0.002)	22	PB	147	2241	1.12
	68	CB	471.75	2268	1.51		29	PB	57.6	2079	1.04
	82	CB	444	2772	1.85		35	PB	252	2490	1.25
	94	PB	130.8	1917	1.28		39	PB	302.25	3003	1.50
	114	CB	222.4	2457	1.64		45	CB	588	4800	2.40
	120	PB	225	2457	1.64		57	PB	112.8	2079	1.04
	143	CB	633.6	3600	2.40		63	PB	413.4	3276	1.64
	156	PB	83.33	2268	1.51		68	PB	360.4	3003	1.50
	168	PB	225	2457	1.64		73	PB	239.2	2490	1.25
	184	CB	448	3300	2.20		78	PB	426	3600	1.80
	191	PB	154	1704	1.14		84	PB	137.9	2079	1.04
(8, 0.0015)	78	PB	137.2	1608	1.07		90	PB	512.4	3900	1.95
	123	CB	240	1917	1.28		95	PB	152.1	2079	1.04
	129	CB	1275.1	4914	3.28		100	PB	282	2739	1.37
	146	PB	88.2	1848	1.23		108	PB	228.6	2490	1.25
	201	PB	89.4	1992	1.33	(9, 0.002)	18	PB	195.3	2988	1.49
	220	CB	278	2349	1.57		23	PB	282.72	3315	1.66
	249	CB	293.33	2490	1.66		34	PB	126	2988	1.49
	317	PB	72	1704	1.14		39	PB	172.8	3060	1.53
	411	PB	35	1608	1.07		45	PB	333.3	3510	1.76
	423	PB	112	2268	1.51		53	PB	446.4	3780	1.89
(9, 0.0015)	31	CB	216	3300	2.20		64	PB	695.6	5625	2.81
	53	PB	64.8	2241	1.49		77	PB	422.4	3600	1.80
	57	PB	89.25	2430	1.62		82	PB	472.2	3900	1.95
	64	PB	72	2295	1.53		85	PB	547.8	4200	2.10
	74	PB	251	2970	1.98		94	PB	566.8	5250	2.63
	90	CB	1520	4500	3.00		103	PB	355.3	3900	1.95
	103	PB	370.8	3300	2.20		110	PB	280.8	2970	1.49
	120	CB	318.5	3960	2.64		113	PB	216	2805	1.40
	126	PB	143.85	2970	1.98		122	PB	418	3510	1.76
	134	PB	273.6	3135	2.09		126	PB	296.4	3060	1.53
	141	PB	136.8	2700	1.80		132	PB	62.4	2739	1.37
	155	PB	146.4	2700	1.80		138	PB	73.6	2805	1.40
	163	PB	81.9	2241	1.49	(5, 0.0025)	15	PB	60	2646	1.06
	212	PB	378	2970	1.98		18	CB	1554.8	5040	2.02
(10, 0.0015)	24	CB	525	3663	2.44		29	PB	263.25	3195	1.28
	37	CB	1584	4500	3.00		37	PB	532.4	3780	1.51
	57	PB	78	3000	2.00		56	PB	402.6	3888	1.56
	62	CB	420	4125	2.75		62	PB	529.2	4032	1.61
	72	CB	225	3663	2.44		68	PB	484.8	3402	1.36
	76	PB	210.6	2700	1.80		71	PB	335.4	2982	1.19
	78	CB	432	4125	2.75		74	PB	385	2982	1.19
	93	PB	132	3750	2.50		79	PB	698	4536	1.81
	108	PB	302.1	3330	2.22		87	PB	112.8	3024	1.21
	174	PB	198.9	3000	2.00		92	PB	488.8	4131	1.65
(12, 0.0015)	19	CB	568	3996	2.66		103	PB	708.4	4284	1.71
	32	CB	1860	4875	3.25		106	PB	279	2982	1.19

(-To be continued-)

(-Continued-) **Table 2** All partial and complete blockages for each experiment

(θ, Q_o) (°, m³/s)	t(s)	TB	V_m (cm³)	Q_{out} (cm³)	m	(θ, Q_o)	t(s)	TB	V_m (cm³)	Q_{out} (cm³)	m
	43	PB	400.8	3663	2.44		117	PB	236.8	2769	1.11
	60	PB	408.8	2997	2.00		121	PB	338.8	3621	1.45
	70	PB	400.8	3330	2.22		13	PB	48	2772	1.11
	74	PB	277.95	2400	1.60		18	PB	332.1	3486	1.39
	85	PB	708.4	3375	2.25		25	PB	466.2	3984	1.59
	98	PB	460.8	2400	1.60		29	CB	1232	6000	2.40
	15	PB	256.1	2664	1.78		41	PB	479.6	3984	1.59
	23	PB	368.2	3375	2.25		49	PB	229.6	3003	1.20
	35	PB	725.76	3540	2.36		52	PB	711.47	4914	1.97
(15, 0.0015)	38	PB	1248.8	3750	2.50		57	PB	270	3237	1.29
	54	PB	130.5	2664	1.78	(7, 0.0025)	60	PB	737.1	4914	1.97
	64	PB	273	2997	2.00		63	PB	649.4	4641	1.86
	80	PB	110.25	2400	1.60		67	PB	639.6	4641	1.86
	92	PB	77	2400	1.60		69	PB	174.4	3003	1.20
	101	PB	143	2997	2.00		72	PB	492	3735	1.49
	46	CB	600	3159	1.58		75	PB	152.6	3237	1.29
	74	PB	132	2343	1.17		78	PB	54.4	2772	1.11
(5, 0.002)	95	CB	842.4	3195	1.60		80	PB	73.8	2772	1.11
	141	PB	549	2343	1.17		84	PB	264	3822	1.53
	179	PB	627	2916	1.46						

Notes: (θ, Q_o) represents the initial conditions of each test, θ is the slope angle, Q_o is the inflow discharge, t is the time when the landslide dam formed after the start of the tests, V_m is the material volume of the landslide dam, Q_{out} is the peak discharge caused by the failure of the landslide dam, m is the coefficient of peak discharge amplification. TB =Types of blockage; PB=partial blockage; CB=complete blockage.

(2) All of the landslide dams that blocked the flume were subdivided into two broad classes: complete blockage and partial blockage. This classification allowed for providing more information in terms of geo-hazard prevention and mitigation.

(3) To analyze the amplification effect of the peak discharge caused by the failure of the landslide dams quantitatively, the coefficient of peak discharge amplification was defined as

$$m = \frac{Q_{out}}{Q_{in}} \tag{1}$$

where m is the coefficient of peak discharge amplification, Q_{in} is the inflow discharge (m³/s), and Q_{out} is the peak discharge downstream of the mine waste accumulations (m³/s). The dimensions of mine waste accumulations can be measured by using the size scale marked on the flume (in Figure 5) and right side tempered glass. Thus the variation of volume of mine waste accumulations in the process of experiments, which is exactly the material volume of the landslide dam, can be calculated based on the videos provided by three cameras. We calibrated the methods before our experiments, and the average error was less than 10%. Table 2 lists all partial and complete blocking for each experiment.

2.1 Amplification effect caused by the failure of landslide dams

In the 13 flume tests, the size, width, height, formation, and failure time of all landslide dams were measured using the size scale marked on the flume by analyzing the videos recorded by the three cameras capturing images from the front, right side, and top of the apparatus. The depth and velocity of each outburst discharge were also measured from the videos. Using the values of the parameters mentioned above, the landslide volume, the outburst discharge, and the amplification coefficient were then calculated. This analysis found that the amplification effects caused by the failure of both complete and partial blockages were significant during the experiments.

Figure 6 shows the evolution of the peak discharge amplification coefficient during the tests with slope angles of 7 and 9 degrees and an inflow discharge of 0.0015 m³/s. In Figure 6, the black symbols indicate the amplification effect caused by

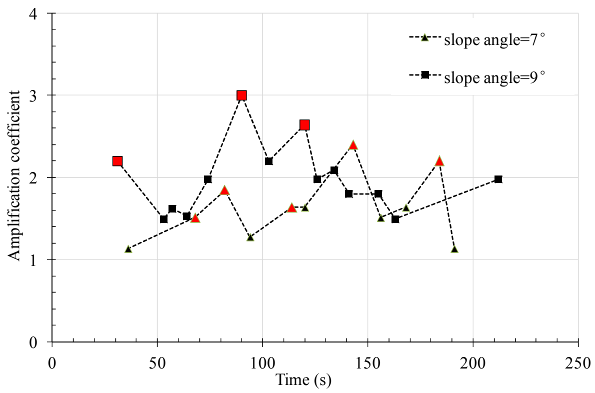

Figure 6 Evolution of peak discharge during the delivery of mine waste (Q_o=0.0015 m³/s).

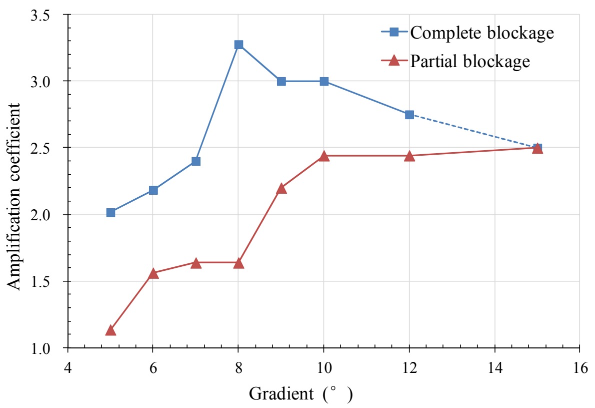

Figure 7 Flume gradient evolution of the amplification coefficient of peak discharge caused by failure of complete and partial blockages.

the failure of partial blockage dams, while the red symbols indicate the amplification effect caused by the failure of complete blockage dams. In general, the damming and breaching effect caused by the failure of a complete blockage is more significant than from a partial blockage. In order to reflect this phenomenon more intuitively, the maximum of the peak discharge amplification coefficient caused by either complete or partial blockages in every test was calculated in Table 2. In the flume tests, there was no complete blockage for the experiments with the initial conditions of Q_o=0.0015 m³/s, θ=15° and Q_o=0.002 m³/s, θ=9°. There were two complete blockages under the initial conditions of Q_o=0.002 m³/s, θ=5° and only a single complete blockage under the initial conditions of Q_o=0.002 m³/s, θ=7° and Q_o=0.0025 m³/s, θ=5° and Q_o=0.0025 m³/s, θ=7°. To make the statistical data comparable, the maximum value of the amplification coefficient caused by one blocking event in each experiment for initial experimental conditions of Q_o of 0.0015 m³/s and θ of 5°, 6°, 7°, 8°, 9°, 10°, 12°, and 15°, were shown in Figure 7 (the value can be looked up in Table 2). From the figure, we can draw the following observations: (1) The outburst discharges caused by the failure of completely blocked landslide dams are much larger than the outburst discharges from partial blockage under the same experimental conditions. (2) The amplification effect of the peak discharge caused by the failure of a complete blockage increases rapidly with increasing flume gradient to a peak reached at θ=8°, then peak decreases with increasing flume gradient. (3) The amplification effect of the peak discharge caused by the failure of a partial blockage always increases with increasing flume gradient, but there is a clear inflection point at a slope of 8°. (4) As the inflow discharge or flume gradient increases, it becomes more difficult to form a complete blockage.

From the perspective of geo-hazard prevention and mitigation, the gully slope and upstream flow rate are two extremely critical parameters when the conditions of the source materials along the gully remain unchanged. The scale and risk of the disaster do not always increase with an increase in the channel gradient; instead, the most unfavorable slope angle happens to be the most favorable slope for the formation of completely blocked landslide dams. In addition, the scale and risk of disaster do not increase with increasing upstream flow rate. Whether or not there is an amplification effect caused by the failure of completely blocked landslide dams is the key to providing an accurate disaster risk assessment. Thus, further exploration of the formation conditions of landslide dams triggered by the incision of mine waste accumulations is required.

2.2 Formation conditions for a complete blockage

Currently, the geomorphic approach is widely used to correlate dam, river, and water-storage characteristics with a landslide dam's formation and stability (Swanson et al. 1986; Costa and Schuster 1988; Casagli and Ermini 1999; Ermini and Casagli 2003; Korup 2004). Casagli and Ermini (1999) proposed two indexes (blockage index and impounding index) to predict and assess the stability of landslide dams. Taking into account the limitations of the parameters involved with the blockage index as defined, only their impoundment index was used to analyze the data from the experiments in this work and to compare them with measured data from actual landslide dams to test the representativeness and reliability of the model experiments. The impoundment index I_i can be defined as:

$$I_i = \log(V_D V_L^{-1}) \quad (2)$$

where V_D is the volume of the landslide dam (m^3) and V_L is the volume of the dammed lake (m^3). Korup (2004) compiled data on 54 existing lakes created by landslide dams and a further 8 breached lakes, which collapsed quickly once formed. The I_i values for these 62 lakes were calculated according to Equation (2) and are shown in Figure 8.

As we can see from Figure 8, the I_i values of naturally formed dammed lakes are mostly between -1 and 3. In addition, the I_i values of existing lakes are all greater than 1 while the I_i values for breached lakes are all less than 1. When the value of I_i is between -1 and 1, it is difficult to determine the stability of the landslide dam according to the I_i value. In this work, there were 28 instances of a complete blockage occurring and then failing by overtopping quickly in the flume tests. Considering the model experiments were scaled with a model scale of 1:100, the scaling must be taken into consideration when compared to the relevant data from actual dammed lakes. Figure 8 also shows the I_i values calculated for the complete blockages in the flume tests, and all of them are concentrated between -1 and 0, which is consistent with natural conditions. The impoundment index I_i thus appears to be a good index for simulating the ratio between the "removing" and "resisting" forces of landslide dams. The former are aptly represented by the volume of impoundage V_L, whereas V_D reflects the magnitude of the geomorphic barrier.

However, the impoundage V_L can neither truly reflect the hydrodynamic conditions of the upstream flow, nor can it explain the phenomenon where the increase of inflow discharge or flume gradient past a certain value actually makes it more difficult to form a complete blockage. Therefore, the stream power, which is a more integrative parameter to represent upstream hydrodynamic conditions, is more suitable, and defined as (Sklar and Dietrich 1998):

$$\Omega = \rho_f g S Q_w \quad (3)$$

where Ω is stream power, ρ_f is fluid density, S is channel slope, and Q_w is the dominant discharge

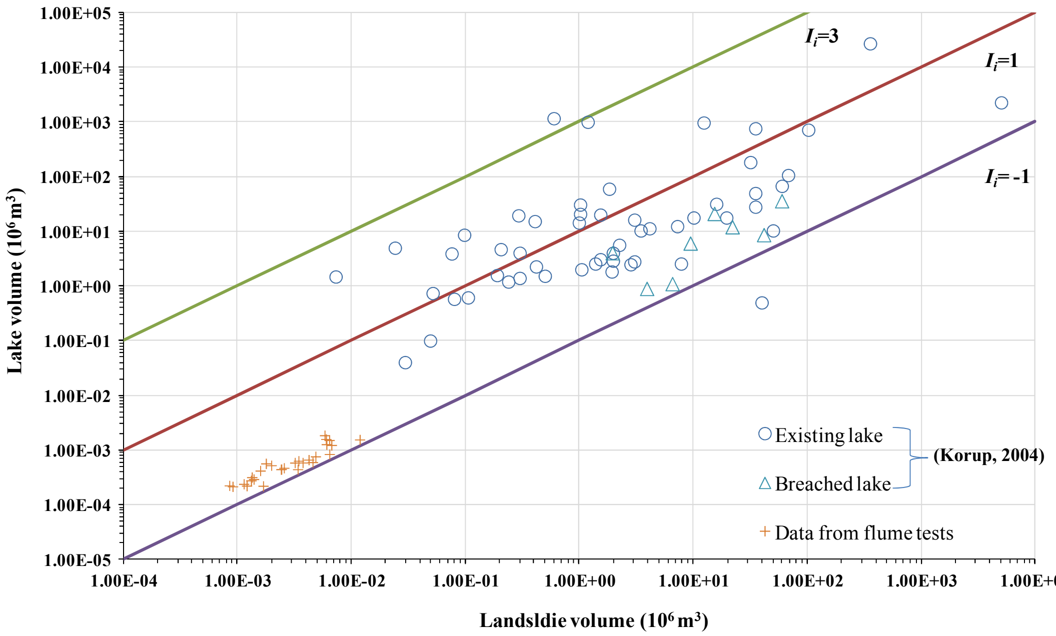

Figure 8 Bivariate plots of landslide dam parameters and graphic envelope curves for impoundment index I_i.

of an unspecified recurrence interval and which can sometimes be replaced by the average discharge.

While the blockage index defined by Casagli and Ermini (1999) was not suitable for this current work, the idea of using such an index to assess the level of blockage is still useful. Instead, we define here a new blockage index based on the stream power, written as:

$$I_{bs} = \log(\rho_s g S Q_w / V_D) \quad (4)$$

where I_{bs} is the blockage index, V_D is the volume of the landslide dam (m^3). Some may consider that it is more reasonable to select the velocity or runout distance rather than the volume of the landslide. Legros (2002) collated information on 203 long-runout landslides that have occurred all over the world and found that the runout distance essentially depends on the volume, and that there is a positive correlation between the velocity and volume of the landslide. Therefore, it is more reasonable to use the volume of the landslide in Equation (4).

There were 28 instances of complete blockage and 122 instances of partial blockage in the 13 tests conducted in this work. However, it can be seen from Equation (4) that I_{bs} is not dimensionless. In order to make the research results more available to be confirmed against field data in future research efforts, it is necessary to adjust the experimental data to match the prototype model scale (1:100) and adopt SI units for further analysis. These analysis results are shown in Figure 9. As can be seen from Figure 9, all of the landslide dams are in the form of a partial blockage when I_{bs} is larger than 4.3, while all of the landslide dams are in form of a complete blockage when I_{bs} is smaller than 3.7. The landslide dams may be in the form of a complete or partial blockage when the value of I_{bs} is between 3.7 and 4.3. The threshold value of the blockage index for a complete blockage was around I_{bs}=4.0.

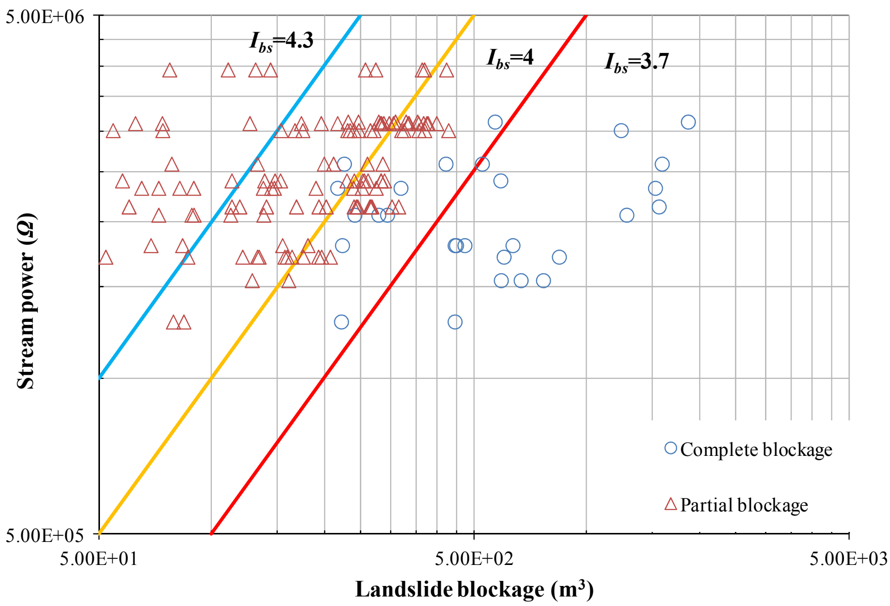

Figure 9 Bivariate plots of landslide dam parameters and graphic envelope curves for blockage index I_{bs}.

2.3 Discussion

In this paper, a new blockage index was developed to represent the degree of blockage. It was found that the threshold value of the blockage index for a complete blockage was around I_{bs}=4.0. In fact, similar research can be found in previous literature. Canuti et al. (1998) proposed a blockage index expressed as follows:

$$I_{bs} = \log(V_D / A_b) \quad (5)$$

Where V_D is the dam volume (m^3) and A_b the upstream catchment area at the point of blockage (km^2). Tacconi et al. (2016) proposed two new indexes, the *MOI* and *HDSI*. These two new indexes were expressed as follows:

$$MOI = \log(V_D / W_v) \quad (6)$$

$$HDSI = \log(V_D / \Omega) = \log(V_D / A_b \cdot S) \quad (7)$$

Where V_D represents the landslide volume (m^3), W_v the width of the dammed valley (m), A_b the catchment area upstream of the blockage point (km^2) and S the local longitudinal slope of the channel bed. Canuti et al. (1998) pointed out that Equation (6) was focused on the dam formation and Equation (7) was focused on the dam stability. The bivariate plots of landslide dam parameters and flume gradient for types of blockage based on the experimental data in Table 2 was shown in Figure 10. It can be seen that the formation conditions for a complete blockage varied with the variation of flume gradient and landslide volume. However, the hydrodynamic conditions, including channel gradient and flow discharge, didn't been considered in Equation (5) and (6). Therefore, Equation (5) and (6) cannot explain the phenomenon where the increase of inflow discharge or flume gradient past a certain value actually makes it more difficult to form a complete blockage (in Figures 7 and 10).

It can be found that *HDSI* was reciprocal of I_{bs} proposed by us in Equation (4). Tacconi et al. (2016) emphasized importance of the stream power (Ω) to stability of the landslide dams. However, a simplified geomorphological formulation was adopted to calculate the stream power as follows:

$$\Omega = A_c \cdot S \quad (8)$$

Compared Equation (8) with Equation (4), it can be found that Equation (8) cannot represent the stream power correctly especially in different rainfall conditions. In addition, these two equations are incomparable as they have different dimensions. Unfortunately, we can rarely capture the hydrological data of the river basin involved with naturally formed landslide dams and cannot calculate the corresponding stream power. As a result, these research results cannot be checked against actual data. In addition, due to the limitations of experimental conditions, the distribution of test points is still relatively narrow. Conditions outside these test points remains a topic for further study.

The new blockage index developed in this work is a more integrative parameter that simulates the ratio between the "removing" and "resisting" forces of landslide dams. What's more, these results suggest that I_{bs} can not only reflect the formation conditions of landslide dams, but also reflect the erosion and delivery rate of dam materials. That is, the faster the erosion rate, the faster the dam failure. This can be seen in the relationship between I_{bs} and the peak discharge amplification coefficient m, which is shown in

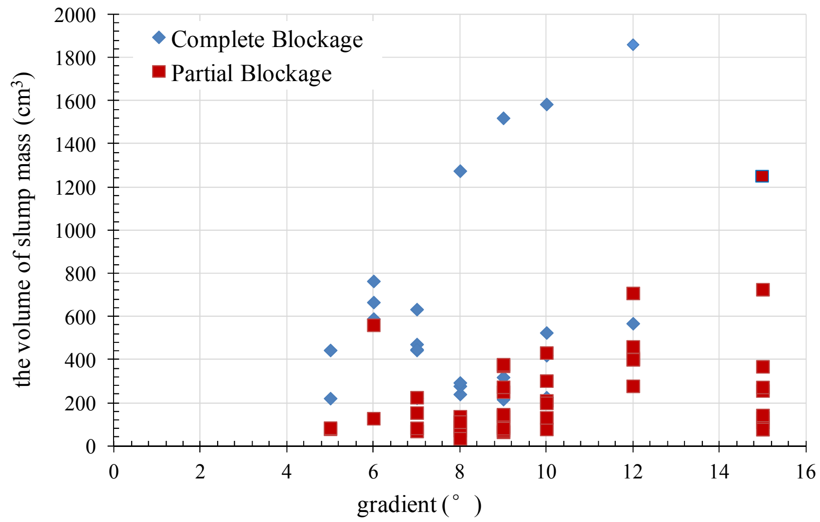

Figure 10 Bivariate plots of landslide dam parameters and flume gradient for types of blockage

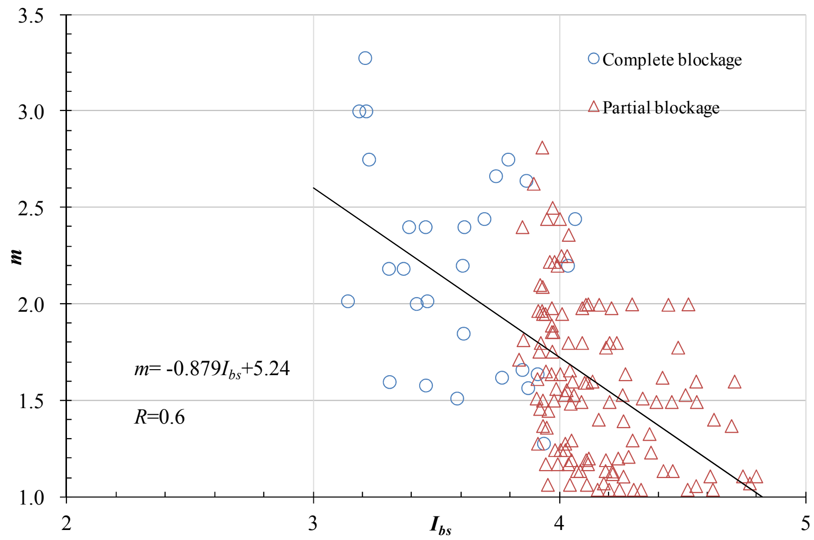

Figure 11 Correlation between blockage index I_{bs} and peak discharge amplification coefficient m.

Figure 11. Note that the two values have a significant negative correlation, with an R of 0.6.

The formation and failure of landslide dams is a complicated process. Due to the limitations of the developed model, only a qualitative analysis of the formation conditions of landslide dams in the process of mine waste erosion and delivery was possible. Our research at this stage was only a preliminarily study to provide a critical value of I_{bs} based on experimental tests. The flume was only 0.3 meters in width and the experimental data must be affected by the side wall boundary effects inevitably. Moreover, Froudian model scaling laws can only maintain dynamic flow similarity and there must be a difference between the prototype and the model. Therefore, the research results still need to be verified against a large amount of actual measurement data in future research efforts.

3 Conclusions

In this paper, the erosion and delivery process of mine waste accumulations was reproduced through flume tests under 13 different sets of experimental condition. From analysis of the results of the flume tests, the following conclusions can be drawn.

(1) Different scale debris slides, induced by the incision of mine waste accumulations, slipped into the channel and caused complete or partial blockages. The failure of these temporary landslide dams amplified the peak discharge significantly. However, the failures of complete blockages have more significant effects on peak discharge amplification than partial blockages. The amplification effect of the peak discharge caused by the failure of a complete blockage increases rapidly with increasing flume gradient to a peak reached at θ=8°, then decreases with increasing flume gradient. As the inflow discharge or flume gradient increases, it becomes more difficult to form a complete blockage.

(2) Based on experimental data, a new blockage index (I_{bs}) was developed to represent the degree of blockage. It was found that all landslide dams formed a partial blockage when I_{bs} was larger than 4.3, while all of the landslide dams formed a complete blockage when I_{bs} was smaller than 3.7. Both partial and complete blockage landslide dams formed when the value of I_{bs} was between 3.7 and 4.3. The threshold value of the blockage index for a complete blockage was around I_{bs}=4.0.

(3) The new blockage index I_{bs} is a more integrative parameter that simulates the ratio between the "removing" and "resisting" forces of landslide dams. There is also a negative correlations between I_{bs} and the peak discharge amplification coefficient m with an R of 0.6.

Acknowledgments

The authors acknowledge the financial support from the National Natural Science Foundation of China (Grant No. 41790441, 41877249 and 41402255) and Shaanxi Natural Science Foundation Project (Grant No. 2017JM4008). Finally, the authors thank Dr. MA Penghui for his kind assistance with the flume experiments.

References

Brown RJ, Rogers DC (1977) A simulation of the hydraulic events during and following the Teton Dam failure. Proceedings of Dam-Break Flood Routing Model Workshop, Bethesda, Maryland, 18-20, October , 131-163.

Canuti P, Casagli N, Ermini L (1998) Inventory of landslide dams in the Northern Apennine as a model for induced flood hazard forecasting. In: Andah, K. (Ed.), Managing Hydro-geological Disasters in a Vulnerable Environment for Sustainable Development CNR-GNDCI Publication CNR-GNDCI-UNESCO (IHP), Perugia. 1900: 189-202.

Casagli N, Ermini L (1999) Geomorphic analysis of landslide dams in the northern Apennine. Transactions of the Japanese Geomorphological Union 20(3): 219-249. https://flore.unifi.it/handle/2158/206201#.XBIVl7xOnLA

Cenderelli DA, Kite JS (1998) Geomorphic effects of large debris flows on channel morphology at North Fork Mountain, Eastern West Virginia, USA. Earth Surface Processes and Landforms 23(1): 1-19. https://doi.org/10.1002/(sici)1096-9837(199801)23:1<1::aid-esp814>3.0.co;2-3

Chen HY, Cui P, Zhou GD, et al. (2014) Experimental study of debris flow caused by domino failure of landslide dams. International Journal of Sediment Research 29(3): 414-422. https://doi.org/10.1016/S1001-6279(14)60055-X

Costa JE, Schuster RL (1988) The formation and failure of natural dams. Bulletin of the Geological Society of America 100(7): 1054-1068. https://doi.org/10.1130/0016-7606(1988)100<1054:TFAFON>2.3.CO;2

Costa JE, Schuster RL (1991) Documented historical landslide dams from around the world. US Geological Survey Open-File Report 91–239. https://doi.org/10.3133/ofr91239

Cui P, Gordon GD, Zhu XH, et al. (2013) Scale amplification of natural debris flows caused by cascading landslide dam failures. Geomorphology 182: 173-189. https://doi.org/10.1016/j.geomorph.2012.11.009

Cui Y, Chan D, Nouri A (2017a) Discontinuum Modeling of Solid Deformation Pore-Water Diffusion Coupling. International Journal of Geomechanics 17(8): 04017033. https://doi.org/10.1061/(ASCE)GM.1943-5622.0000903

Cui Y, Chan D, Nouri A (2017b) Coupling of Solid Deformation and Pore Pressure for Undrained Deformation – a discrete Element Method Approach. International Journal for Numerical and Analytical Methods in Geomechanics 41(18): 1943-1961. https://doi.org/10.1002/nag.2708

Cui Y, Nouri A, Chan D, et al. (2016) A new approach to the DEM simulation of sand production. Journal of Petroleum Science and Engineering 147: 56-67. https://doi.org/10.1016/j.petrol.2016.05.007

Deng LS, Fan W, Xiong W, et al. (2009) Development features and risk of inducing slag debris flow at Daxicha Gully. Journal of Engineering geology 17(3): 415-420. (In Chinese). https://doi.org/10.1016/S1003-6326(09)60084-4

Dong JJ, Tung YH, Chen CC, et al. (2009) Discriminant analysis of the geomorphic characteristics and stability of landslide dams. Geomorphology 110(3-4): 162-171. https://doi.org/10.1016/j.geomorph.2009.04.004

Ermini L, Casagli N (2003) Prediction of the behavior of landslide dams using a geomorphological dimensionless index. Earth Surface Processes and Landforms 28(1): 31-47. https://doi.org/10.1002/esp.424

Fread DL (1977) The development and testing of a dam-break flood forecasting model, Proceedings of Dam-Break Flood Routing Model Workshop, Bethesda, Maryland, 18-20, October. 164-197. https://doi.org/10.1117/12.871960

Gallino GL, Pierson TC (1984) The 1980 Polallie Creek debris flow and subsequent dam-break flood, East Fork Hood River Basin, Oregon. U.S. Geological Survey Open-File Report 84: 578. https://doi.org/10.3133/ofr84578

Hu W, Xu Q, Rui C, et al. (2015) An instrumented flume to investigate the initiation mechanism of the post-earthquake huge debris flow in southwest of China. Bulletin of Engineering Geology and the Environment 74 (2): 393-404. https://doi.org/10.1007/s10064-014-0627-3

Legros F (2002) The mobility of long-runout landslides. Engineering geology 63(3-4): 301-331. https://doi.org/10.1016/S0013-7952(01)00090-4

King J, Loveday I, Schuster RL (1989) The 1985 Bairaman landslide dam and resulting debris flow, Papua New Guinea. Quarterly Journal of Engineering Geology 22(4): 257–270. https://doi.org/10.1144/GSL.QJEG.1989.022.04.02

Korup O (2002) Recent research on landslide dams-a literature review with special attention to New Zealand. Progress in Physical Geography 26: 206-235. https://doi.org/10.1191/0309133302pp333ra

Korup O (2004) Geomorphometric characteristics of New Zealand landslide dams. Engineering Geology 73: 13-35. https://doi.org/10.1016/j.enggeo.2003.11.003

Korup O (2005) Geomorphic hazard assessment of landslide dams in South Westland, New Zealand: fundamental problems and approaches. Geomorphology 66(1-4): 167-188. https://doi.org/10.1016/j.geomorph.2004.09.013

Li ZS (1995) A study on the mud rock flow disaster in 1994 in the gold mine area of Tongguan, Shaanxi. Journal of Catastrophology 10(3): 51-56. (in Chinese)

Liu SJ, Xie H, Wei FQ, et al. (1996) A man-caused debris flow in Xiaoqinling Gold Mining region. Mountain Research, 14(4): 259-263. (In Chinese). https://doi.org/10.16089/j.cnki.1008-2786.1996.04.011

Lombard RE, Miles MB, Nelson LM, et al. (1981) The impact of mudflows on May 18 on the lower Toutle and Cowlitz Rivers. The 1980 eruptions of Mount St. Helens, Washington. U.S. Geological Survey Professional Paper 1250: 693–699.

Ponce VM, Yevjevich V (1978) Muskingum-Cunge method with variable parameters. Journal of hydraulics Division 104(12): 1663-1667.

Straub S (1997) Predictability of long runout landslide motion: implications from granular flow mechanics. Geologische Rundschau 86(2): 415-425. https://doi.org/10.1007/s005310050150.

Stefanelli CT, Samuele S, Casagli N, et al. (2016) Geomorphic indexing of landslide dams evolution. Engineering Geology 208: 1-10. https://doi.org/10.1016/j.enggeo.2016.04.024.

Schuster RL (2000) Outburst debris flows from failure of natural dams. Proceedings 2nd International Conference on Debris Flow Hazard Mitigation. 16-20, August, Taipei, 29–42.

Singh VP, Scarlatos PD, Jourdan MR, et al. (1986) Simulation aspects of earth dam failures. In G A Keramides and Brebbia (eds), Computational Methods and Experimental Measurements, Springer-Verlag, New York. 263-273.

Sklar L, Dietrich WE (1998). River longitudinal profiles and bedrock incision models: stream power and the influence of sediment supply. In: Tinkler KJ, Wohl EE (Eds.), Rivers Over Rock. Fluvial Processes in Bedrock Channels. Washington D.C. 237-260. https://doi.org/10.1029/GM107p0237.

Swanson FJ, Oyagi N, Tominaga M (1986) Landslide dam in Japan. In: Schuster, R.L.(Ed.), Landslide Dam: Processes Risk and Mitigation. American Society of Civil Engineers. Geotechnical Special Publication 3: 131-145.

Zhou GD, Cui P, Chen HY, et al. (2013) Experimental study on cascading landslide dam failures by upstream flows. Landslides 10: 633-643. https://doi.org/10.1007/s10346-012-0352-6